processes

MDPI

Article

A New Approach to the Preparation of Stable Oxide-Composite Cobalt–Samarium Catalysts for the Production of Hydrogen by Dry Reforming of Methane

A. G. Dedov [1,2], A. S. Loktev [1,2,*], V. A. Arkhipova [2], M. A. Bykov [3], A. A. Sadovnikov [1], K. A. Cherednichenko [2] and G. A. Shandryuk [1]

[1] A. V. Topchiev Institute of Petrochemical Synthesis, Russian Academy of Sciences, Leninsky Prosp. 29, 119991 Moscow, Russia; dedov.a@gubkin.ru (A.G.D.); sadovnikov@ips.ac.ru (A.A.S.); gosha@ips.ac.ru (G.A.S.)

[2] Chair of General and Applied Chemistry, National University of Oil and Gas «Gubkin University», Leninsky Prosp. 65, 119991 Moscow, Russia; nlaaln2015@gmail.com (V.A.A.); cherednichenko.k@gubkin.ru (K.A.C.)

[3] Department of Chemistry, Lomonosov Moscow State University, Leninskie Gory 3/1, 119991 Moscow, Russia; mich.bykov@gmail.com

* Correspondence: al57@rambler.ru or genchem@gubkin.ru

Abstract: A new approach to preparing a series of Co/Sm_2O_3 catalysts for hydrogen production by the dry reforming of methane has been developed. The catalyst precursors were synthesized with a simple method, including the evaporation of aqueous solutions of cobalt and samarium nitrates, followed by a short-term calcination of the resulting material. The as-prepared and spent catalysts were characterized using X-ray diffraction, scanning electron microscopy, transmission electron microscopy, temperature-programmed reduction, and thermogravimetric analysis. The content of cobalt in the synthesized materials affects their phase composition and carbonization resistance in the dry reforming of the methane reaction. It has been shown that preheating in N_2 atmosphere produces catalysts that provide a stable yield of hydrogen and CO of 94–98% for at least 50 h at 900 °C. These yields are among the highest currently available for the dry reforming of methane catalysts made from Co-Sm complex oxides. It has been established that the decrease in the amount of cobalt in the catalyst and its preheating to an operating temperature of 900 °C in a nitrogen flow help to prevent the carbonization of the catalyst and the sintering of metal particles.

Keywords: heterogeneous catalysis; hydrogen; syngas; dry reforming of methane; cobalt–samarium oxide catalysts

Citation: Dedov, A.G.; Loktev, A.S.; Arkhipova, V.A.; Bykov, M.A.; Sadovnikov, A.A.; Cherednichenko, K.A.; Shandryuk, G.A. A New Approach to the Preparation of Stable Oxide-Composite Cobalt–Samarium Catalysts for the Production of Hydrogen by Dry Reforming of Methane. *Processes* **2023**, *11*, 2296. https://doi.org/10.3390/pr11082296

Academic Editor: Davide Papurello

Received: 3 July 2023
Revised: 27 July 2023
Accepted: 28 July 2023
Published: 31 July 2023

1. Introduction

The increasing threat of global climate change has prompted the governments of 195 countries to adopt the "Paris Agreement", which aims to reduce greenhouse gas emissions, primarily by decarbonizing the economy [1,2]. In this regard, hydrogen is considered the most environmentally friendly alternative fuel since its combustion is accompanied only by the release of water vapor into the air. Hydrogen has the highest energy intensity per unit mass but low density. In addition to being a promising fuel, hydrogen is used in increasing amounts in ammonia synthesis and oil refining, and as a synthesis gas (syngas) component for the production of methanol and a number of other petrochemicals [1–4].

The main industrial process of hydrogen production is the steam reforming of methane (1), which is a high-energy endothermic process requiring the production and consumption of a considerable amount of water vapor [2,5,6].

$$CH_4 + H_2O \rightleftharpoons CO + 3H_2 \; \Delta H^0_{298} = +206 \text{ kJ} \quad (1)$$

Promising processes for hydrogen production from methane are the partial oxidation of methane, POM, (2), and dry reforming of methane, DRM, (3).

$$2CH_4 + O_2 \rightleftharpoons 2CO + 4H_2 \; \Delta H^0{}_{298} = -36 \text{ kJ} \quad (2)$$

$$CH_4 + CO_2 \rightleftharpoons 2CO + 2H_2 \; \Delta H^0{}_{298} = +247 \text{ kJ} \quad (3)$$

Since reaction (2) is exothermic, the POM process, in combination with the steam reforming of methane, is implemented in the autothermal mode. In addition, POM allows the production of syngas (H_2:CO = 2:1), suitable for direct processing into petrochemical products [5–8]. The practical application of POM is largely limited by the need to use pure oxygen, which causes an explosion hazard, and the possible sintering of metal active centers when "hot spots" appear in the catalyst bed.

The process of hydrogen production by DRM reaction has been extensively studied in recent decades. For example, the number of publications on this topic in 1990–2022 exceeded 1000, including 863 scientific articles with more than 6 citations, and 34 reviews [9]. The growing interest in this topic is due to several factors. The first factor is the aforementioned efforts of most countries to reduce the greenhouse effect [1–3]. The DRM process allows the utilization of both methane and carbon dioxide, the most common greenhouse gases after water. Secondly, the DRM process is a way to produce hydrogen and other valuable products by processing renewable raw materials, biogas, i.e., it represents a promising decarbonization strategy [10]. Thirdly, the industrial process of hydrogen production by the steam reforming of methane includes an additional stage of the steam reforming of CO (4):

$$CO + H_2O \rightleftharpoons CO_2 + H_2 \quad (4)$$

The CO_2 generated from this process also needs to be recovered, and it can be involved in the DRM process as a raw material.

In addition, the joint methane steam reforming and DRM can also be used for the utilization of CO_2 captured from the flue gases of methane steam reforming plants [2]. Finally, the DRM process also produces syngas, which is a suitable intermediate for the synthesis of dimethyl ether, hydrocarbons through the Fischer–Tropsch process, etc. [1–4,6,9,11–16]. Furthermore, the syngas from the DRM process can be used in fuel cells [13].

As for the use of the DRM process, this process has been implemented mainly on a pilot scale, and in combination with the steam reforming of methane to control the composition of the resulting syngas [15–18]. The process [15–17,19], known as CALCOR, primarily aims to obtain carbon monoxide (H_2:CO = 0.42:1) and, therefore, it is accomplished with a large excess of CO_2. The industrial implementation of DRM is constrained by several features of this process, such as high endothermicity associated with the stability of CO_2 and CH_4 molecules, "sintering" of active catalyst centers associated with a high temperature of the process, and a significant formation of coke deposits. It was shown that the DRM process conducted at elevated pressures is accompanied by an enhanced carbonization of catalysts. Therefore, a costly stage of compression will be necessary for the syngas produced by DRM, which is required for subsequent processing [1,13,15,17,20–22]. A high temperature of the process also requires complex hardware design.

According to thermodynamic calculations, DRM does not produce a high yield of syngas at low temperatures. To achieve its high yields by reaction (3) at H_2:CO = 1:1, with the reagent conversion close to 100% and reduced carbon formation by the methane pyrolysis reaction (5), a ratio of CO_2:CH_4 = 1:1, a temperature above 850 °C, and atmospheric pressure are required [12,13,16,17,22–25].

$$CH_4 \rightleftharpoons C + 2H_2 \; \Delta G^0{}_{298} \leq 0 \text{ at } T \geq 658 \text{ C}. \quad (5)$$

These conditions also favor the reverse water gas shift reaction (6), which affects the ratio of DRM products and the value of CO_2 conversion:

$$CO_2 + H_2 \rightleftharpoons CO + H_2O\ \Delta G^0{}_{298} \leq 0 \text{ at } T \geq 700 \text{ C}. \quad (6)$$

Carbon formation in the DRM process is possible not only by reaction (5), but also by the disproportionation of CO (7), and the hydrogenation of CO (8) and CO_2 (9) [12,26].

$$2CO \rightleftharpoons C + CO_2\ \Delta H^0{}_{298} = -172 \text{ kJ} \quad (7)$$

$$CO + H_2b \rightleftharpoons C + H_2O\ \Delta H^0{}_{298} = -131 \text{ kJ} \quad (8)$$

$$CO_2 + 2H_2 \rightleftharpoons C + 2H_2O\ \Delta H^0{}_{298} = -90 \text{ kJ} \quad (9)$$

However, these reactions are exothermic, thermodynamically unfavorable at high temperatures, and probably proceed in the opposite direction.

One of the key approaches to the practical implementation of the DRM process considered in most relevant publications is to design selective, stable, and resistant to carbonization catalysts. The objectives are to prevent sintering of the active centers of catalysts and the formation of stable forms of surface carbon (graphite, carbon fibers, and nanotubes), which deactivate active centers, destroy the catalyst, and block the passage of gases through a reactor. Complex oxides of the perovskite structure are commonly in use as promising DRM catalysts [1–3,5,6,10–15]. As a result of pre-reduction or contact with reagents, the perovskite structure of catalysts is transformed, forming composites containing a highly dispersed metal phase in an oxide matrix. In some cases, such systems demonstrate high activity, selectivity, and stability in DRM. In these compounds, the catalysts are based on nickelates and cobaltates of rare earth elements [5,11,27–33]. According to these studies, the perovskite precursors of catalysts can be synthesized with various methods, such as solid-phase synthesis, self-propagating high-temperature synthesis, sol-gel synthesis, the decomposition of specially synthesized complex compounds, etc. The choice of the synthesis method largely determines the properties of the DRM catalysts.

The aim of the present study is to find optimal conditions for the preparation of highly efficient, stable, and resistant to carbonization Co/Sm_2O_3 catalysts with various cobalt content for hydrogen production by DRM.

2. Materials and Methods

2.1. Materials

We used the following commercial Sigma-Aldrich reagents: $Co(NO_3)_2 \bullet 6H_2O$ CAS 10026-22-9, and $Sm(NO_3)_3 \bullet 6H_2O$ CAS 13759-83-6.

2.2. Preparation of Catalyst

The designations of the synthesized materials—catalysts precursors—and the amounts of reagents used for their synthesis are given in Table 1. The amounts of reagents corresponded to the cobalt content in the resulting catalyst (Table 1). $Co(NO_3)_2 \bullet 6H_2O$ and $Sm(NO_3)_3 \bullet 6H_2O$ were dissolved in 30 mL of distilled water under stirring in a glass beaker. The obtained solutions were heated under stirring until water evaporation. The resulting mass was transferred into an alundum crucible and heated in a Nabertherm (Nabertherm GMBH, Lilienthal, German) muffle furnace for 3 h at 300 °C. The solid product was crushed, heated in air in the muffle furnace for 2.5 h to 800 °C, and kept for 2 h at this temperature.

Table 1. The code of catalysts, the mass of reagents taken for the synthesis of catalysts and the specific surface area (S_{BET}) of the materials obtained.

Code of Catalysts	Mass of $Co(NO_3)_2 \bullet 6H_2O$, g	Mass of $Sm(NO_3)_3 \bullet 6H_2O$, g	S_{BET}, m^2/g
2% Co/Sm_2O_3	0.49	12.49	2
5% Co/Sm_2O_3	1.23	12.11	3
10% Co/Sm_2O_3	2.47	11.47	4
23% Co/Sm_2O_3	2.91	4.47	4

2.3. Characterization of Catalysts

The specific surface area S_{BET} of the samples was measured by the method of low-temperature nitrogen adsorption on an ATKh-06 analyzer (Katakon, Novosibirsk, Russia). The samples were degassed in a nitrogen flow (1 atm) at 200 °C for an hour prior to analysis. Based on the data obtained, the specific surface area of the samples was calculated using the Brunauer–Emmett–Teller (BET) model and the five-points method in the partial pressure range of 0.05–0.25 P/P_0.

The powder X-ray diffraction study (XRD) of freshly prepared and spent catalysts was carried out on a Rigaku MiniFlex 600 (Rigaku, Tokyo, Japan) diffractometer (CuKα radiation, detector with graphite monochromator, and Cu anticathode). The XRD data were processed using the database of the International Center for Diffraction Data (ICDD).

Thermogravimetric analysis (TGA) was performed on a TGA/DSC 3+ simultaneous thermal analyzer (Mettler Toledo), in an air flow in the range of 30–1000 °C at a heating rate of 10 °C/min. The TGA data were processed using the STARe Excellence software SW V16.10.

The micromorphology of all samples was studied by scanning electron microscopy (SEM) on a Carl Zeiss NVision 40 high-resolution microscope (Carl Zeiss, Jena, Germany), equipped with an Oxford Instruments X-MAX detector (80 mm^2) and operating at an accelerating voltage of 1–20 kV. SEM images were taken in InLens (SE2) and ESB modes with an Everhart–Thornley detector, at accelerating voltages of 1 and 7 kV.

The microstructure and elemental mapping of some spent catalysts were investigated on a TJEOL JEM-2100 UHR (JEOL, Tokyo, Japan) transmission electron microscope (TEM), operating at an accelerating voltage of 200 kV. Sample powders were dispersed in ethanol and dropped onto a TEM cooper grid (Ted Pella, Inc., Redding, CA, USA). TEM micrographs were collected in the bright-field mode using an Olympus Quemesa 11-megapixel CCD camera. The dark-field sample images and elemental mapping were performed in the STEM mode.

The temperature-programmed reduction (H_2-TPR) was performed in a flow quartz reactor with an inner diameter of 2 mm at a heating rate of 7.5 °C/min. Temperature was measured with the aid of a chromel–alumel thermocouple (K-type). The velocity of the H_2/Ar flow (5 vol.% H_2) was 50 mL/min. The H_2 content in the outlet gas flow was assessed on a Krystallux-4000M chromatograph equipped with a thermal conductivity detector.

In addition, the H_2-TPR of the catalysts was carried out in the same mode on an USGA-101/M3 chemisorption analyzer (LLC UNISIT, Moscow, Russia).

2.4. Catalytic Experiments

The catalytic performance of 2% Co/Sm_2O_3, 5% Co/Sm_2O_3, 10% Co/Sm_2O_3, 23% Co/Sm_2O_3 materials in the DRM process was tested at atmospheric pressure in a fixed bed flow quartz reactor (inner diameter 18 mm) with an axial pocket for thermocouple (outer diameter 8 mm). The tip of the thermocouple (chromel–alumel (K)) was positioned in the center of the catalyst layer. Powdered catalysts precursors were pressed into pellets, grinded, and, in further experiments, a fraction with a grain size of 0.5–1 mm was used. The catalyst precursor (0.2 g, layer height 1 mm) was placed on a quartz fiber substrate. The catalyst precursor was heated to 900 °C in a nitrogen stream (JSC NIIKM, Moscow,

Russia, nitrogen content 99.999%). After the N_2 supply was stopped, a gas mixture of CH_4 and CO_2 (JSC "Moscow Gas Processing Plant", Moscow, Russia, purity at least 99.9%) was fed into the reactor. The ratio of CH_4:CO_2 was 1, and the feed rate of the nitrogen or gas mixture was 15 L $\times$ g^{-1} $\times$ h^{-1}. The gas velocity at the reactor inlet and outlet was measured with a foam flow meter. The temperature change in the reactor was carried out using a programmable temperature controller. The products were analyzed at a fixed temperature, and the temperature was adjusted to other set values without stopping the supply of reagents.

The composition of gaseous products was analyzed online by GC on GALS 311 chromatographs equipped with thermal conductivity detectors using He as a carrier gas. The concentrations of H_2, CH_4, and CO were estimated at 30 °C in a 2 m $\times$ 3 mm steel column packed with NaX zeolite. The H_2 concentration was calculated using a special calibration graph. To detect CH_4, CO_2, ethylene, and ethane, a similar column filled by a Porapak Q at 70 °C was used. The admixtures of C_{2+} hydrocarbons were determined at 70 °C, using a similar column filled by 5% Na_2CO_3 on alumina. The chromatographic data were analyzed using the EKOCHROM software (SKB of the Zelinsky Institute of Organic Chemistry, Russian Academy of Sciences). All chromatograms were calculated by internal normalization, with correction made for the molecular weights of the components.

Calculations

Methane conversion, X(CH_4), was calculated as:

$$X(CH_4) = \frac{W_{in}(CH_4) - W_{out}(CH_4)}{W_{in}(CH_4)} \times 100\% \quad (10)$$

where $W_{in}(CH_4)$ is the quantity (mol) of CH_4 injected in the reactor and $W_{out}(CH_4)$ is the quantity (mol) of CH_4 at the reactor outlet.

CO_2 conversion X(CO_2) were calculated similarly.

Hydrogen yield, Y(H_2), was calculated as:

$$Y(H_2) = \frac{W_{out}(H_2)}{2W_{in}(CH_4)} \times 100\% \quad (11)$$

where $W_{out}(H_2)$ is quantity (mol) of H_2 at the reactor outlet and $W_{in}(CH_4)$ is the quantity (mol) of CH_4 injected in the reactor.

CO yield, Y(CO), was calculated as:

$$Y(CO) = \frac{W_{out}(CO)}{W_{in}(CH_4) + W_{in}(CO_2)} \times 100\% \quad (12)$$

where $W_{out}(CO)$ is the quantity (mol) of CO at the reactor outlet and $W_{in}(CH_4)$ and $W_{in}(CO_2)$ are the quantities (mol) of CH_4 and CO_2 injected in the reactor, respectively.

3. Results and Discussion

In blank experiments conducted in the reactor without a catalyst, a slight carbonization of reactor walls was detected mainly after a layer of quartz nozzle and quartz fiber. At the same time, the trace amounts of CO and hydrogen were detected in exhaust gases, along with unreacted reagents.

After catalytic experiments, only H_2 and CO, as well as unconverted CH_4 and CO_2, were detected in the exhaust gases. Sometimes traces of H_2O were detected, but special additional experiments are required to correctly determine the total amount of H_2O formed. These experiments were not carried out when performing this work.

3.1. Characterization of Freshly Prepared Materials

According to the XRD data, the synthesized sample of 2% Co/Sm_2O_3 contains phases of Sm_2O_3 (ICDD 96-101-0341, 88 wt.%) and Sm_2CoO_4 (ICDD 96-200-2267, 12 wt.%) (Figure S1a). The phase content was calculated by the Rietveld method [34].

Sample 5% Co/Sm_2O_3 (Figure S1b), along with Sm_2O_3 (ICDD 96-101-0341, 86 wt.%), contains the $SmCoO_3$ phase (ICDD 96-412-4856, 14 wt.%). Sample 10% Co/Sm_2O_3 (Figure S1c) contains Sm_2O_3 (ICDD 99-208-1967, 47 wt.%) and $SmCoO_3$ (ICDD 99-204-5928, 53 wt.%). 23%Co/Sm_2O_3 (Figure S1d), in which the amount of cobalt corresponds to its content in the $SmCoO_3$ perovskite, contains only 35 wt.% of $SmCoO_3$ (ICDD 96-152-1745), in addition to Sm_2O_3 (ICDD 96-101-0590, 42 wt.%) and Co_3O_4 (ICDD 96-153-8532, 23 wt.%). Thus, the samarium/cobalt ratio in the synthesized complex oxides significantly affects their phase composition. XRD patterns of four Co/Sm_2O_3 samples clearly demonstrate the interaction between cobalt and Sm_2O_3 resulted in formation of Sm_2CoO_4 phase in the case of 2% Co/Sm_2O_3 with lowers Co content and $SmCoO_3$ phase in other samples. A higher amount of cobalt in 23% Co/Sm_2O_3 leads to the formation of an additional Co_3O_4 phase.

The SEM images of the synthesized materials (Figure 1a–d) show that all samples are formed by flat particles with an undeveloped porous structure, which corresponds to a low specific surface area of the samples (Table 1).

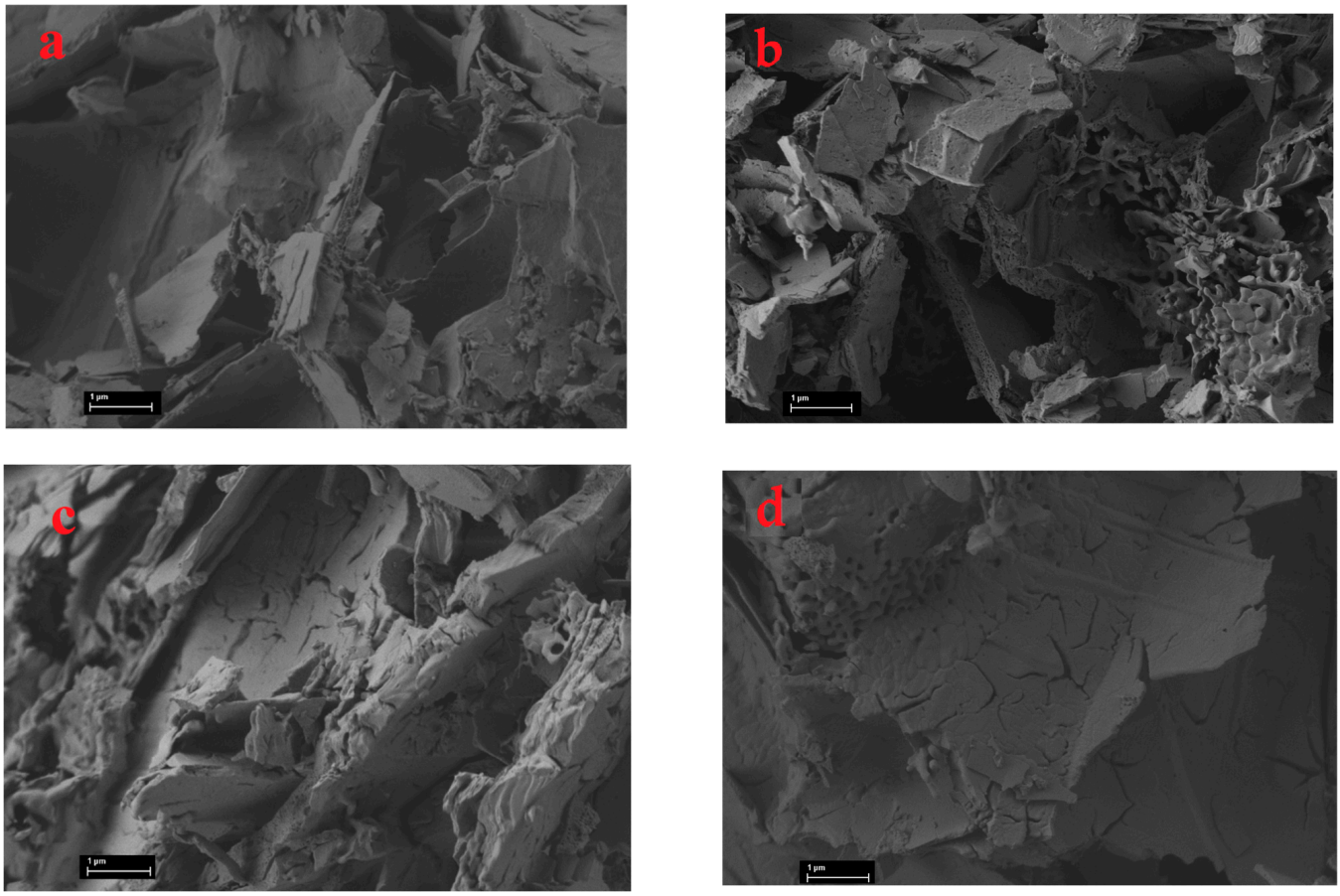

Figure 1. SEM images in SE2 mode of (**a**) 2% Co/Sm_2O_3, (**b**) 5% Co/Sm_2O_3, (**c**) 10% Co/Sm_2O_3, and (**d**) 23% Co/Sm_2O_3.

The H_2-TPR profile of 2% Co/Sm_2O_3 (Figure 2a) reveals the presence of three regions of hydrogen absorption. Low intense peaks with maxima at 310 and 400 °C are probably related to reduction of a small amount of X-ray amorphous Co_3O_4 contained in the catalyst [35], which was not recorded by XRD. An intense peak with a maximum at

540 °C, according to [11,31,36], can be assigned to the reduction of samarium cobaltite by reaction (13):

$$Sm_2CoO_4 + H_2 = Sm_2O_3 + Co + H_2O. \quad (13)$$

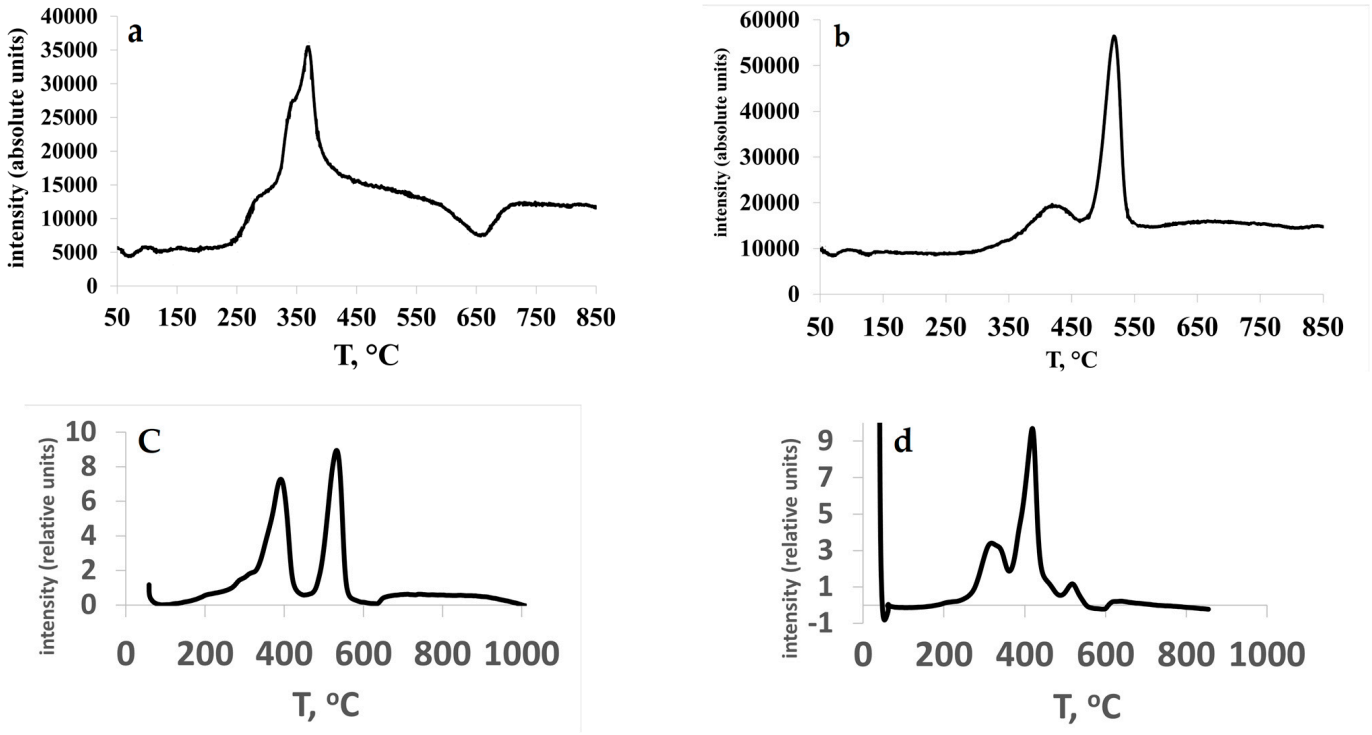

Figure 2. H_2-TPR profiles of (**a**) 2% Co/Sm_2O_3, (**b**) 5% Co/Sm_2O_3, (**c**) 10% Co/Sm_2O_3, and (**d**) 23% Co/Sm_2O_3.

The H_2-TPR profile of 5% Co/Sm_2O_3 (Figure 2b) exhibits a low-intensity peak with a maximum at 420 °C and an intense peak with a maximum at 530 °C, which, according to [11,31,36], can be attributed to the staged reduction of samarium cobaltate by reactions (14) and (15):

$$2SmCoO_3 + H_2 = 2SmCoO_{2.5} + H_2O \quad (14)$$

$$2SmCoO_{2.5} + 2H_2 = Sm_2O_3 + 2Co + 2H_2O \quad (15)$$

The H_2-TPR profiles of 10% Co/Sm_2O_3 (Figure 2c) and 23% Co/Sm_2O_3 (Figure 2d) were recorded by the USGA analyzer. The H_2-TPR profile of 10%Co/Sm_2O_3 shows two intense peaks with maxima at 390 and 532 °C, which, according to [11,31,36], can also be attributed to the staged reduction of samarium cobaltate by reactions (14) and (15).

The H_2-TPR graph of 23% Co/Sm_2O_3 exhibits a peak with a maximum at 318 °C, corresponding to the reduction of cobalt oxides, and an intense peak with a maximum at 419 °C, which can be assigned to the reduction of both cobalt oxides and samarium cobaltate by reaction (14). A less intense peak with a maximum at 517 °C probably corresponds to reaction (15). In general, the H_2-TPR data obtained for the synthesized samples are consistent with the XRD analysis (Figure S1a–d and comments).

3.2. Results of Catalytic Experiments

In our recent work, lanthanum nickelate [30] and samarium cobaltate [29] perovskites were prepared by the thermal decomposition of specially synthesized heterometallic complex compounds $(M^1(phen)_x][M^2(NO_3)_y(H_2O)]\cdot zMeCN$, where M^1 is Ni or Co, M^2 is La or Sm, phen is o-phenanthroline, and MeCN is methyl acetate). These compounds served as precursors of efficient DRM catalysts, which are composites containing metallic nickel or

cobalt dispersed in a matrix of lanthanum or samarium oxides. However, during the DRM process, despite the thermodynamically favorable conditions, their surface was subjected to significant carbonization, which led to blockage of the gas flow in the reactor. Using a complex procedure of the supercritical antisolvent deposition of a complex compound—the precursor of perovskite $SmCoO_3$, the catalyst particle size was decreased, and catalyst carbonization was avoided [29].

However, we have shown that the production of efficient DRM catalysts does not require the mandatory synthesis of a completely single-phase initial perovskite [37,38]. Composites containing, along with the perovskite phase, the phases of nickel, cobalt, and rare earth elements oxides can be synthesized using a simple evaporation of aqueous solutions of nickel, cobalt, and rare earth elements (REE) salts. In the DRM process, these composites form catalysts consisting of metallic nickel or cobalt dispersed in an REE oxide. These catalysts make it possible to obtain syngas with a yield above 90%, but undergo significant carbonization.

To create a DRM catalyst less susceptible to carburization, an oxide composite containing 2 wt.% cobalt was synthesized by the simple evaporation of an aqueous solution of cobalt and samarium nitrates, followed by calcination of the resulting material at 700 °C [39]. It was assumed that, due to a decrease in the cobalt content in this material compared to the $SmCoO_3$ perovskite containing 23 wt.% cobalt, metallic cobalt particles more resistant to sintering and subsequent carbonization would be obtained. It is known that the deposition of perovskite systems on various substrates often increases their efficiency in DRM catalysis [11,14,16,20]. It was expected that the synthesized material would contain samarium cobaltate $SmCoO_3$ dispersed in a matrix of samarium oxide. However, the formed composite consisted of samarium oxide and samarium cobaltite, Sm_2CoO_4, which apparently resulted from the interaction of $SmCoO_3$ with an excess of samarium oxide.

It was found [39] that this material, after prereduction in CH_4 and CO_2 mixture or in hydrogen flow, formed a catalyst which demonstrated low efficiency in DRM. It showed syngas yields of 88–90% at 900 °C only after a long-term exposure in the CH_4/CO_2 flow.

In the present work, 2% Co/Sm_2O_3 was preheated to 900 °C for an hour in a high-purity nitrogen flow. The results are shown in Figure 3. In contrast to the results presented in [39], immediately after the mixture of CH_4 and CO_2 was fed to the reactor, a yield of the syngas ($CO:H_2$ = 1:1) equal to 96% was achieved. The conversion of CH_4 was 97%, and the conversion of CO_2 was 99%. In a long-term experiment with intermediate cooling and reheating to 900 °C in high-purity nitrogen, the stable performance of the catalyst for 50 h was observed. Since the DRM results presented in [39] demonstrate that, on 2% Co/Sm_2O_3 catalyst, a decrease in temperature leads to a decrease in the conversion of reagents and the yields of products, this catalyst was not tested at temperatures lower than 900 °C. Our results demonstrate that a highly efficient and stable DRM catalyst is formed in situ immediately after the contact of 2% Co/Sm_2O_3 preheated to 900 °C in N_2 flow with the CH_4-CO_2. mixture.

The data in Figure 4 indicate that, for the catalyst derived from 5% Co/Sm_2O_3, the CH_4 conversion is 95–98%, the CO_2 conversion is 100%, the CO yield is 97–98%, and the H_2 yield is 95–97%. When reaction temperature was reduced to 800 °C, the CH_4 conversion decreased to 83–84%, the CO_2 conversion to 90–91%, the CO yield to 81–83%, and the H_2 yield to 82%. At 700 °C, the CH_4 conversion was 46–47%, the CO_2 conversion was 58–59%, the CO yield was 47–49%, and the H_2 yield was 39–41%, while at 600 °C almost no DRM was observed. A subsequent increase in temperature to 900 °C restored the activity of the catalyst. When the experiment was continued up to 50 h, high values of CH_4 conversion (94–96%), CO_2 conversion (99–100%), CO yield (94–97%), and H_2 yield (94–96%) were maintained.

According to Figure 5, the catalyst derived from 10% Co/Sm_2O_3 demonstrates approximately the same results in the DRM reaction as the catalyst derived from 5% Co/Sm_2O_3.

For a comparison, we synthesized a 23% Co/Sm_2O_3 material and tested it in the DRM reaction (Figure 6). The same material was previously tested in the DRM reaction

after preheating in the reagent stream [38]. According to [38], at 900 °C, the formed catalyst shows a syngas yield close to quantitative value, but after a catalytic test it contains 44.5 wt.% of carbon deposits. Taking into account the data from [38] and the tests of catalysts based on 2% Co/Sm_2O_3, 5% Co/Sm_2O_3, and 10% Co/Sm_2O_3 in the present work, this material was tested in the DRM reaction after preheating at 900 °C for an hour in the high-purity nitrogen stream. Figure 6 demonstrates that, during 55 h on stream, the catalyst formed from 23% Co/Sm_2O_3 retained 95–98% CH_4 conversion, 98–100% CO_2 conversion, 95–98% CO yield, and 94–97% H_2 yield.

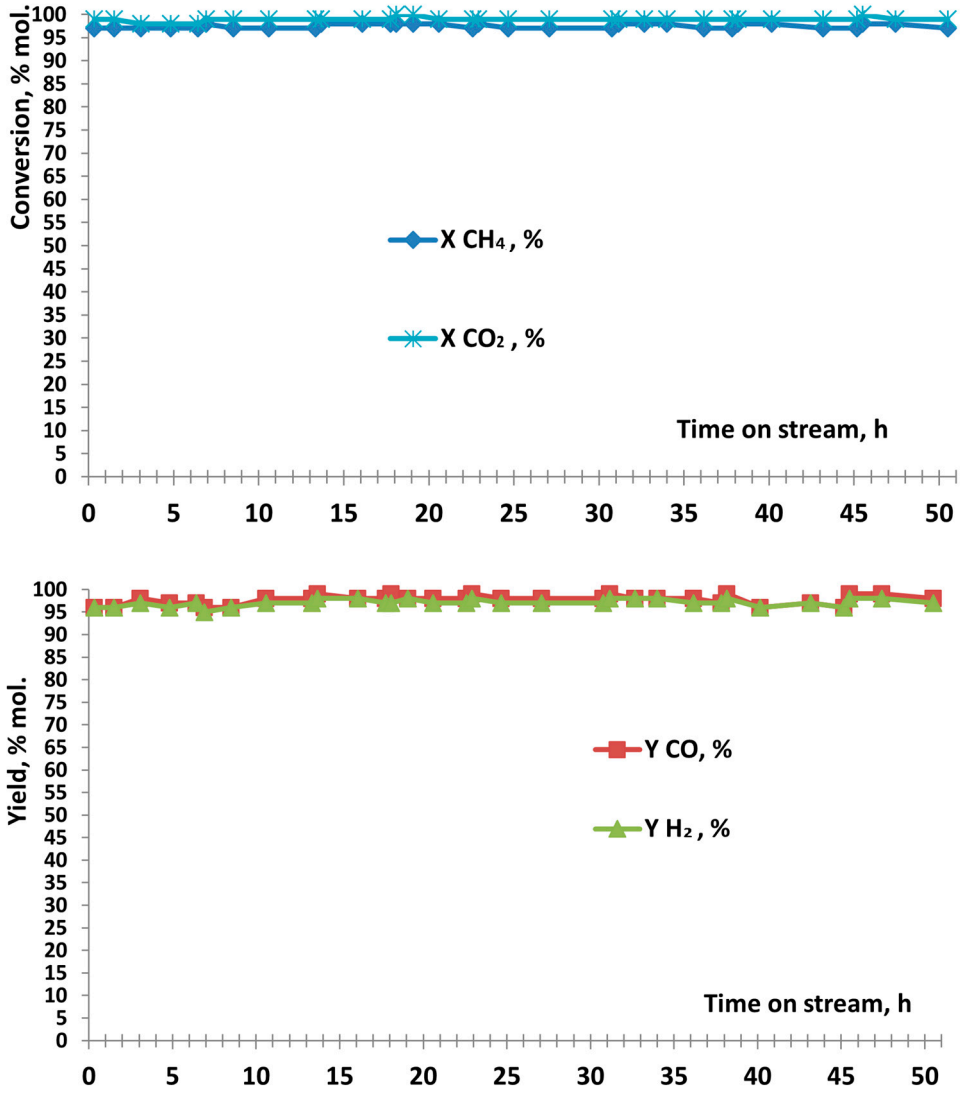

Figure 3. The performance in DRM process of 2% Co/Sm_2O_3 derived catalyst preheated at 900 °C in N_2 flow.

The 5% Co/Sm_2O_3 and 10% Co/Sm_2O_3 samples, which were also preheated at 900 °C for an hour in the high-purity nitrogen flow, as well as the 2% Co/Sm_2O_3 sample, immediately formed catalysts that showed high yields of CO and H_2 (Figures 4 and 5).

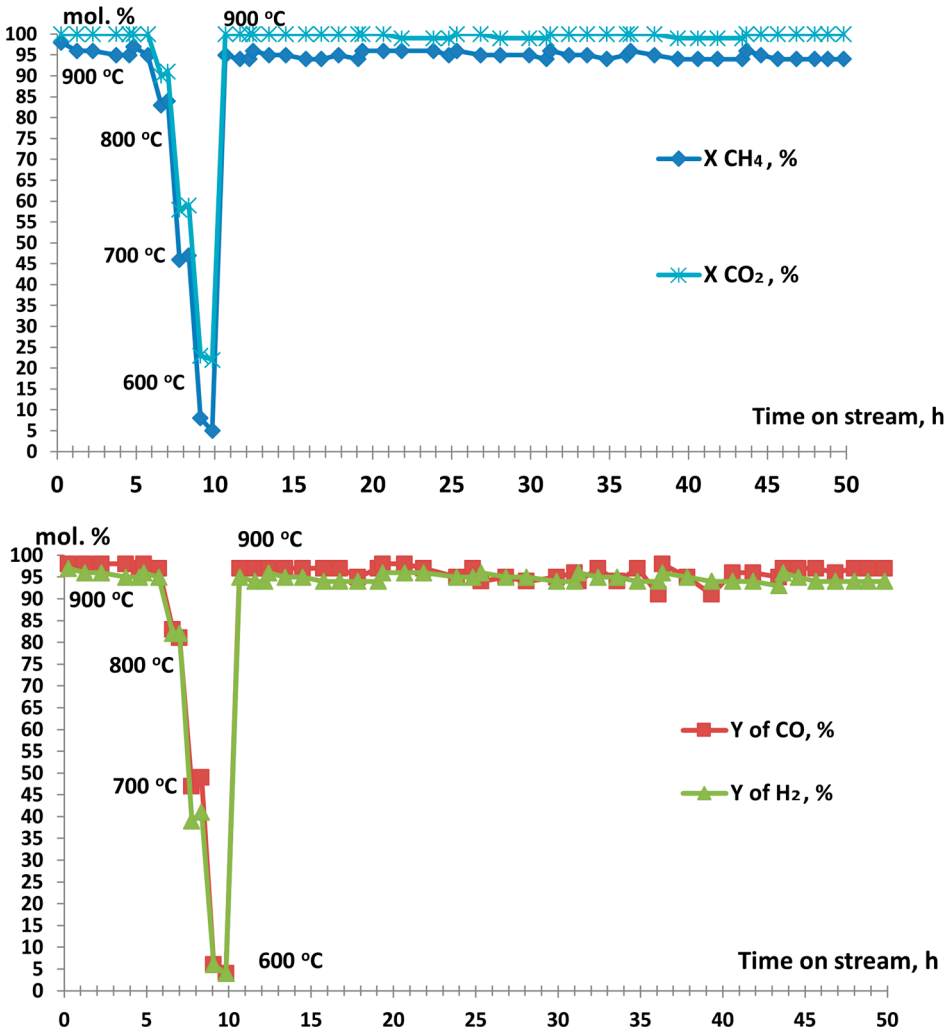

Figure 4. Performance of 5% Co/Sm_2O_3 derived catalyst preheated at 900 °C in N_2 flow in DRM process.

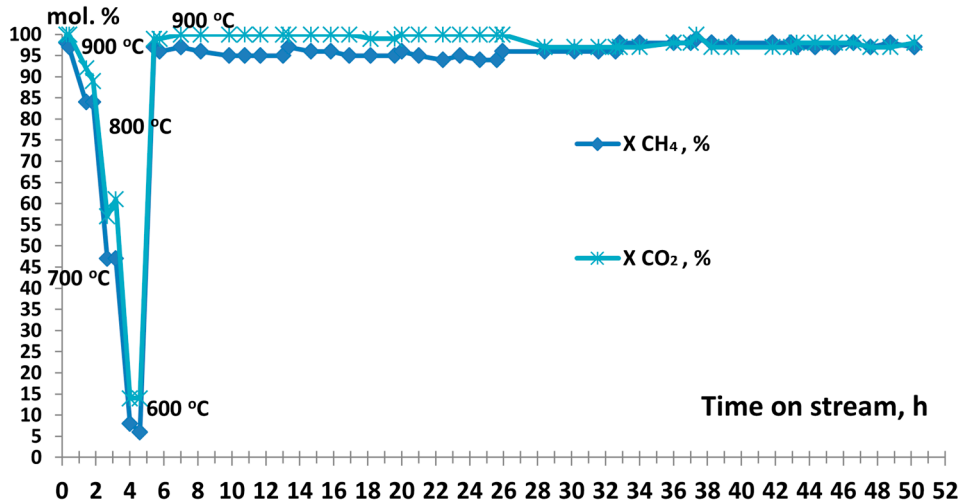

Figure 5. *Cont.*

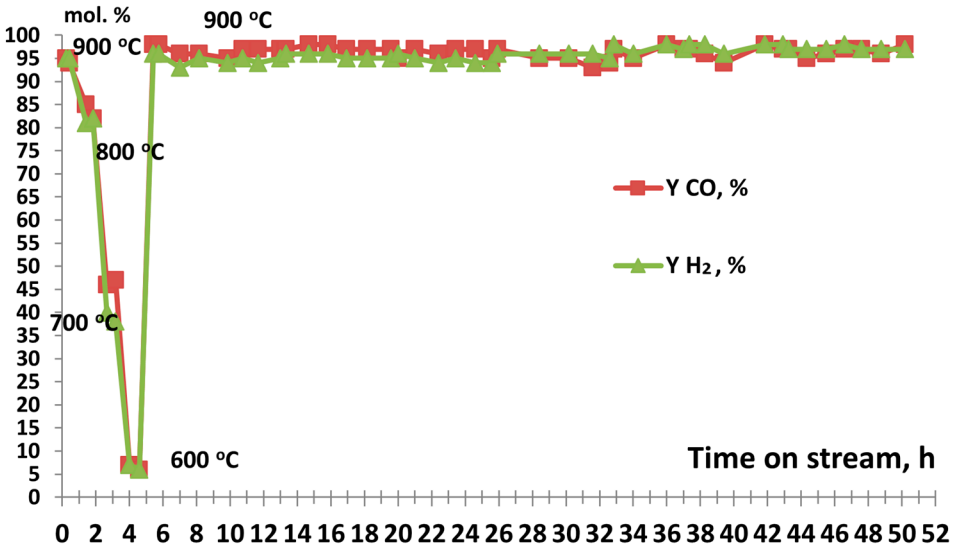

Figure 5. Performance of 10% Co/Sm_2O_3 derived catalyst preheated at 900 °C in N_2 flow in DRM.

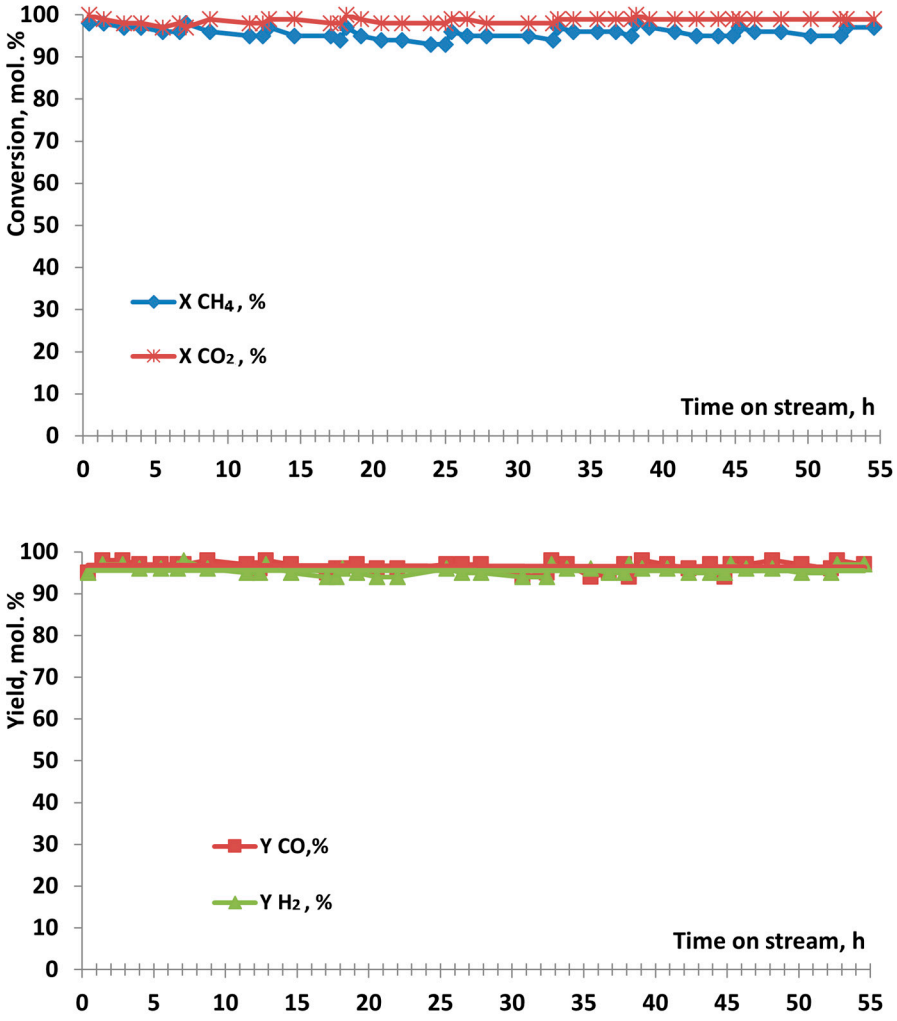

Figure 6. Performance of 23% Co/Sm_2O_3 derived catalyst preheated at 900 °C in N_2 flow in DRM process.

It should be noted that previously studied catalysts derived from 2% Co/Sm_2O_3 [39] and 23% Co/Sm_2O_3 [38] showed a deterioration in the results of the DRM reaction with a decrease in temperature—the same as when testing the catalysts derived from 5% Co/Sm_2O_3 and 10% Co/Sm_2O_3.

The catalysts formed during the DRM process and discharged from the reactor were investigated by XRD, TGA, and TEM methods.

The XRD data of the spent catalysts are shown in Figure S2a–d.

The XRD pattern of the spent catalyst derived from 2% Co/Sm_2O_3 (Figure S2a) shows only reflections of cubic Sm_2O_3 (ICDD 96-101-0590) and rhombic Sm_2O_3 (ICDD 96-153-0725). The absence of reflections of cobalt and its compounds may be explained by the small number of such particles and their small size.

The XRD patterns of the spent catalysts derived from 5% Co/Sm_2O_3 (Figure S2b), 10% Co/Sm_2O_3 (Figure S2c) and 23% Co/Sm_2O_3 (Figure S2d) exhibits reflections corresponding to metallic cobalt, along with reflections of cubic Sm_2O_3 (ICDD 96-901-5549) and rhombic Sm_2O_3. In the case of the spent catalyst derived from 5% Co/Sm_2O_3, a low intensity of reflexes makes it impossible to estimate the size of cobalt particles according to the Debye–Scherrer formula. The spent catalysts derived from 10% Co/Sm_2O_3 and 23% Co/Sm_2O_3, in accordance with the Debye–Scherrer formula, contains cobalt particles of 52–56 nm and 43–48 nm, respectively. Thus, the XRD data (Figure S2b–d) indicate that the evolution of 5% Co/Sm_2O_3, 10% Co/Sm_2O_3, and 23% Co/Sm_2O_3 in the reaction medium provides the formation of composites, including metallic cobalt dispersed in samarium oxide—and it is highly probable these are the true DRM catalysts. As we have already noted above, the absence of reflections of cobalt and its compounds in the XRD pattern of the spent catalyst derived from 2% Co/Sm_2O_3 may be explained by a small Co amount and small size of Co particles. It should be noted that all the formed composites maintain high activity in DRM for at least 50 h.

The TGA data obtained for the spent catalysts are shown in Figure 7a–d.

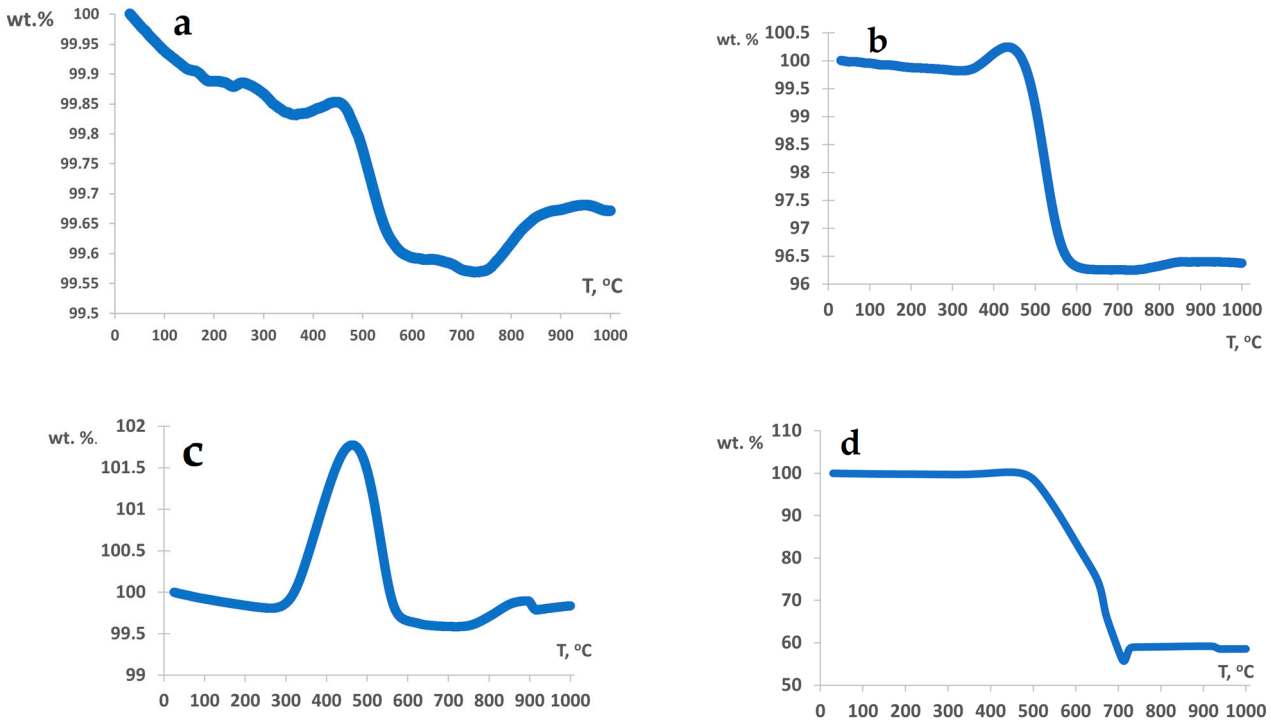

Figure 7. TGA profiles of spent catalysts derived from (**a**) 2% Co/Sm_2O_3, (**b**) 5% Co/Sm_2O_3, (**c**) 10% Co/Sm_2O_3, and (**d**) 23% Co/Sm_2O_3.

All the samples are characterized by a slight initial weight loss associated with the removal of adsorbed water and gases upon heating to 300 °C. At higher temperatures, marked differences in TGA profiles are observed.

The TGA profile of the spent catalyst derived from 2% Co/Sm_2O_3 (Figure 7a) shows that, upon heating from 350 to 450 °C, the weight slightly increases, which is apparently due to the oxidation of metallic cobalt. At 450–650 °C, the weight decreases by 0.26%, which correlates with the combustion of carbonaceous deposits and possibly the decomposition of carbonates admixtures. A slight weight loss at 650–750 °C may be attributed to the combustion of more oxidation-resistant forms of carbon, and a subsequent increase in weight can be explained by the resynthesis of cobalt–samarium complex oxides.

The TGA profiles of other spent catalysts demonstrate variable weight, evidently increasing due to the oxidation of metallic cobalt and decreasing in correlation with the combustion of carbonaceous deposits and the decomposition of carbonates. A subsequent increase in weight is presumably caused by the resynthesis of cobalt–samarium complex oxides.

Thus, the TGA data of all the studied samples indicate the presence of metallic cobalt in the formed composites. The TGA data indicate that the catalyst formed from 2% Co/Sm_2O_3 is practically not subjected to carburization. Catalysts based on 5% Co/Sm_2O_3 and 10% Co/Sm_2O_3 are carbonized to a small extent, whereas the catalyst based on 23% Co/Sm_2O_3 undergoes strong carbonization, although it does not lose activity in DRM for more than 50 h.

The TGA results are consistent with the SEM data (Figure 8a–d).

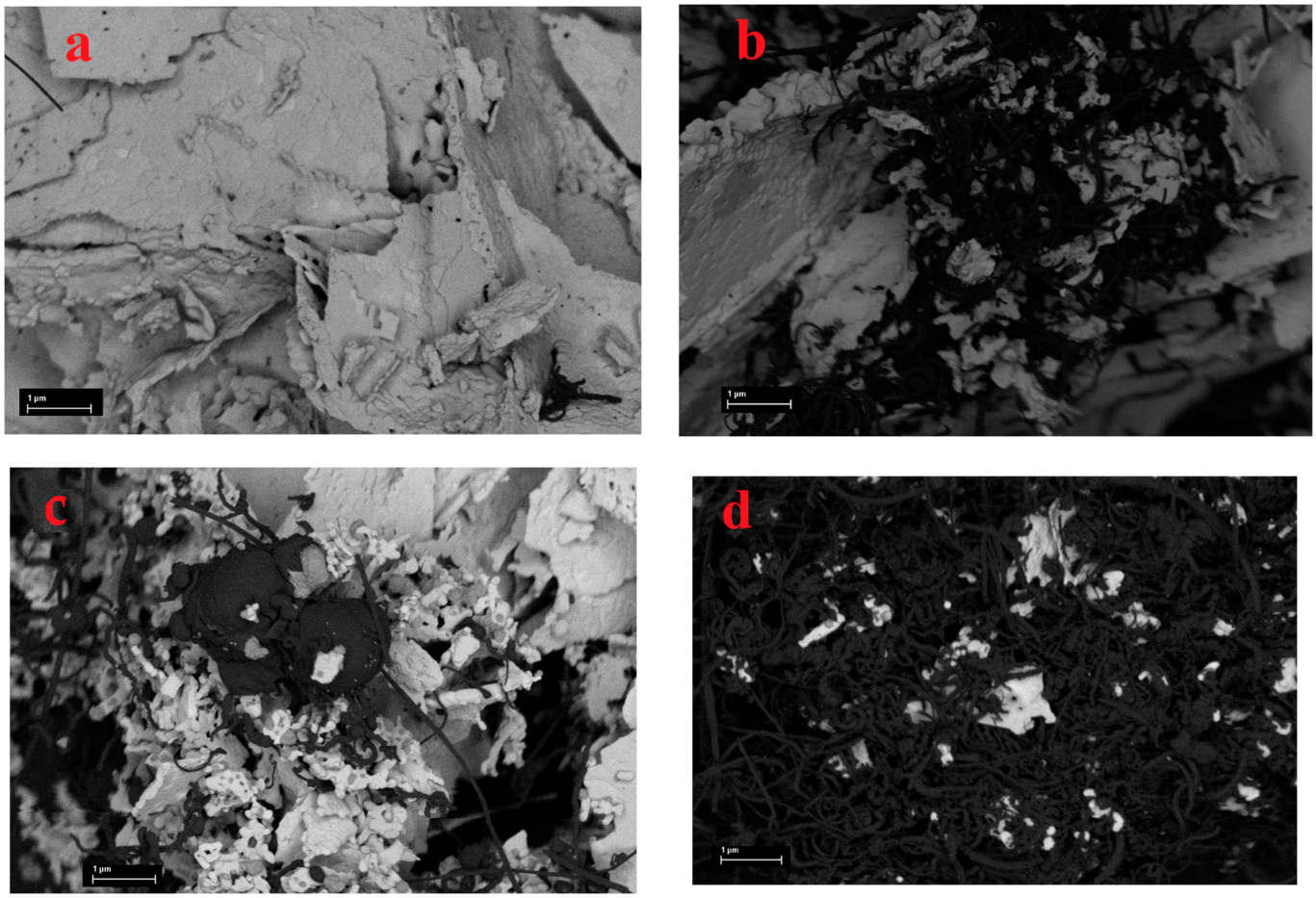

Figure 8. ESB SEM images of spent catalysts derived from (**a**) 2% Co/Sm_2O_3, (**b**) 5% Co/Sm_2O_3, (**c**) 10% Co/Sm_2O_3, and (**d**) 23% Co/Sm_2O_3.

The spent catalyst derived from 2% Co/Sm_2O_3 (Figure 8a) contains almost no carbon deposits. The spent catalysts based on 5% Co/Sm_2O_3 (Figure 8b) and 10% Co/Sm_2O_3 (Figure 8c), underwent noticeable carbonization, and the surface of the spent catalyst derived from 23% Co/Sm_2O_3 (Figure 8d) is almost completely covered with carbon deposits.

Spent catalysts with the lowest cobalt content, which were derived from 2% Co/Sm_2O_3 and 5% Co/Sm_2O_3, were additionally investigated by the TEM method. The TEM micrograph of the spent catalyst based on 2% Co/Sm_2O_3 (Figure 9a) demonstrates the formation of an insignificant amount of carbon nanotubes. Figure 9b shows that the catalyst contains cobalt particles with a size of approximately 20 nm.

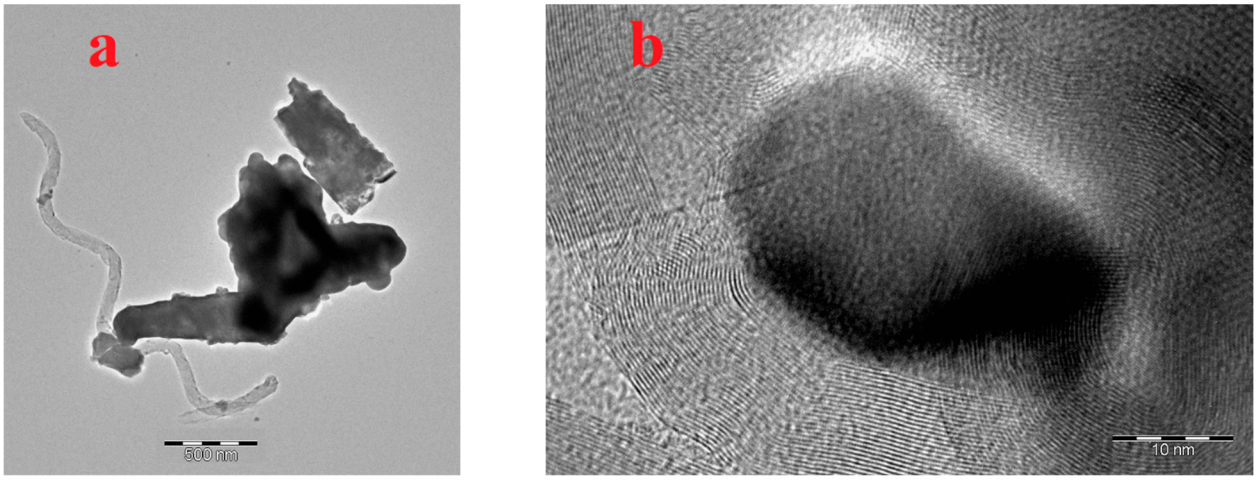

Figure 9. TEM images of spent catalyst derived from 2% Co/Sm_2O_3; (**a**) image of catalyst particle, (**b**) high resolution image of Co particle in the catalyst.

Figure 10 presents the TEM data on the elemental composition and distribution of cobalt and samarium in the spent catalyst derived from 2% Co/Sm_2O_3. It can be seen that cobalt is evenly distributed in samarium oxide.

For a comparison, the spent catalyst derived from 5% Co/Sm_2O_3, which is more prone to carbonization, was also investigated by TEM (Figure 11).

The TEM micrographs show that the sample contains both pure and carbon-covered cobalt particles up to 50 nm in size, as well as non-surface-bound carbon nanotubes. This sample has a higher tendency to coking, which may be explained by an increase in the size of cobalt-containing particles.

The study of the elemental composition of this material (Figure 12) also showed that the regions of cobalt and samarium distribution in the sample are coincident. However, some places with an increased concentration of Co are visible in the cobalt map on Figure 12.

Thus, the simple method of synthesizing catalyst precursors, namely, the evaporation of aqueous solutions of cobalt and samarium nitrates with the subsequent calcination of the resulting material, makes it possible to obtain materials that are precursors of selective and stable catalysts of the DRM reaction. This method is much simpler than most of the known methods used to prepare highly efficient and stable catalysts of this reaction based on cobalt–samarium precursors [7,11,29–31], including single-phase perovskite $SmCoO_3$ [29–31]. The cobalt loading in such precursors affects its phase composition. Namely, according to XRD data, the 2% Co/Sm_2O_3 sample contains Sm_2O_3 and Sm_2CoO_4 phases. Materials based on 5% Co/Sm_2O_3 and 10% Co/Sm_2O_3 contain $SmCoO_3$, along with Sm_2O_3. The 23% Co/Sm_2O_3 sample containing the same amount of cobalt as that which is similar in composition to $SmCoO_3$ perovskite consists of $SmCoO_3$, Sm_2O_3, and Co_3O_4.

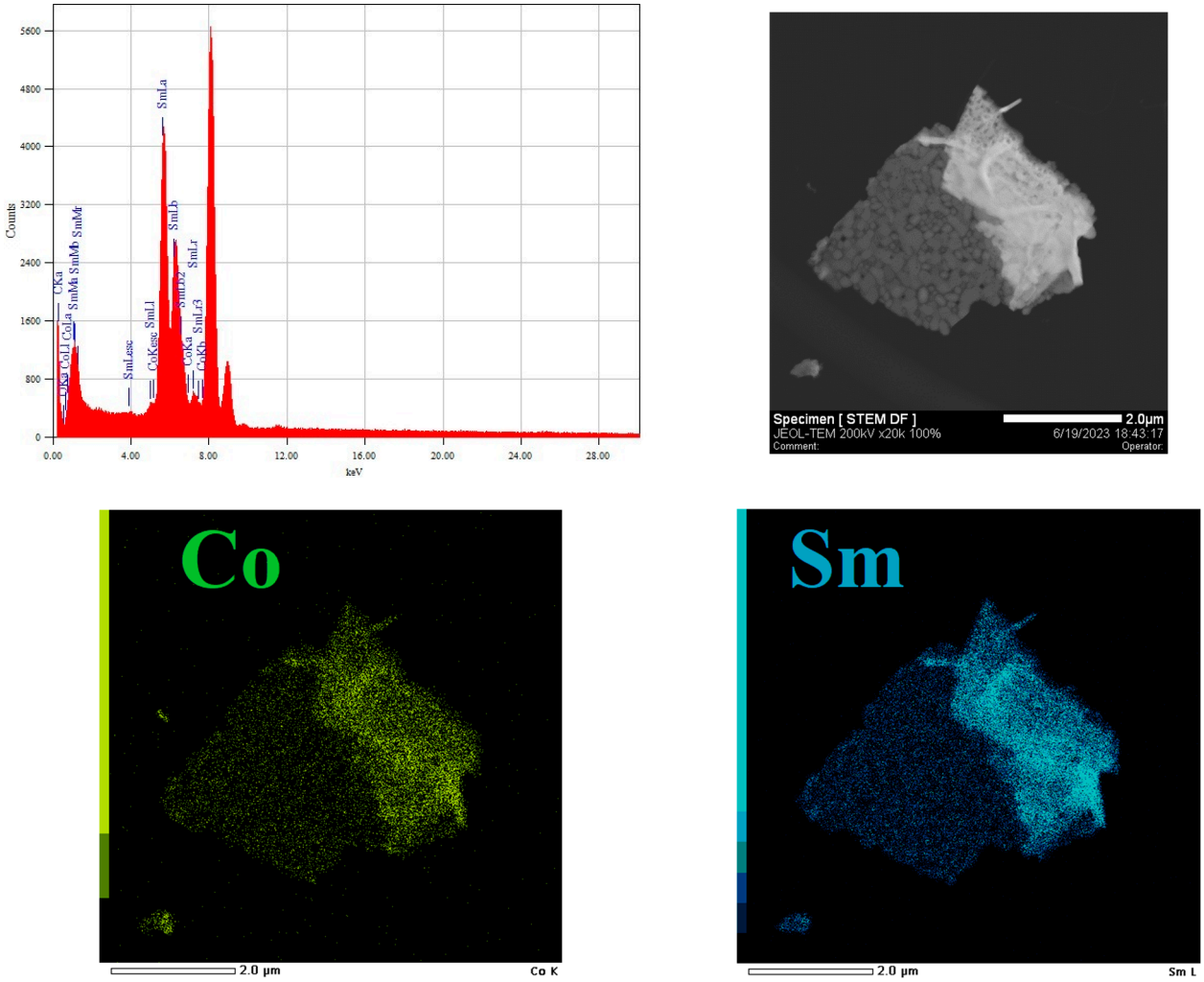

Figure 10. TEM images for the spent catalyst derived from 2% Co/Sm_2O_3: overall elemental spectra, STEM DF image, Co and Sm elemental maps.

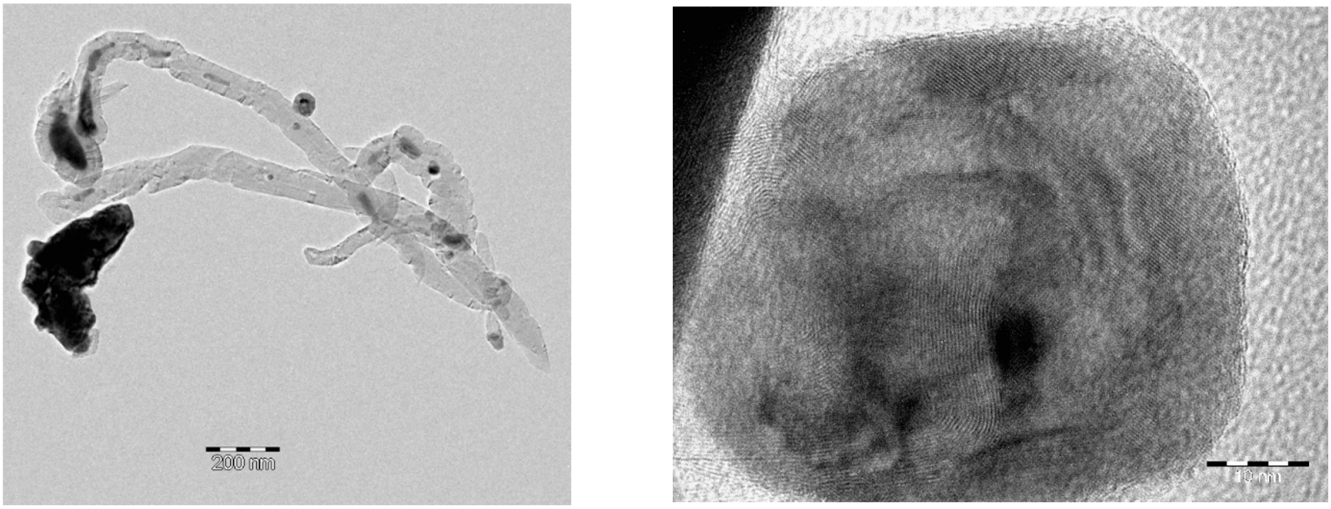

Figure 11. TEM images of spent catalyst derived from 5% Co/Sm_2O_3.

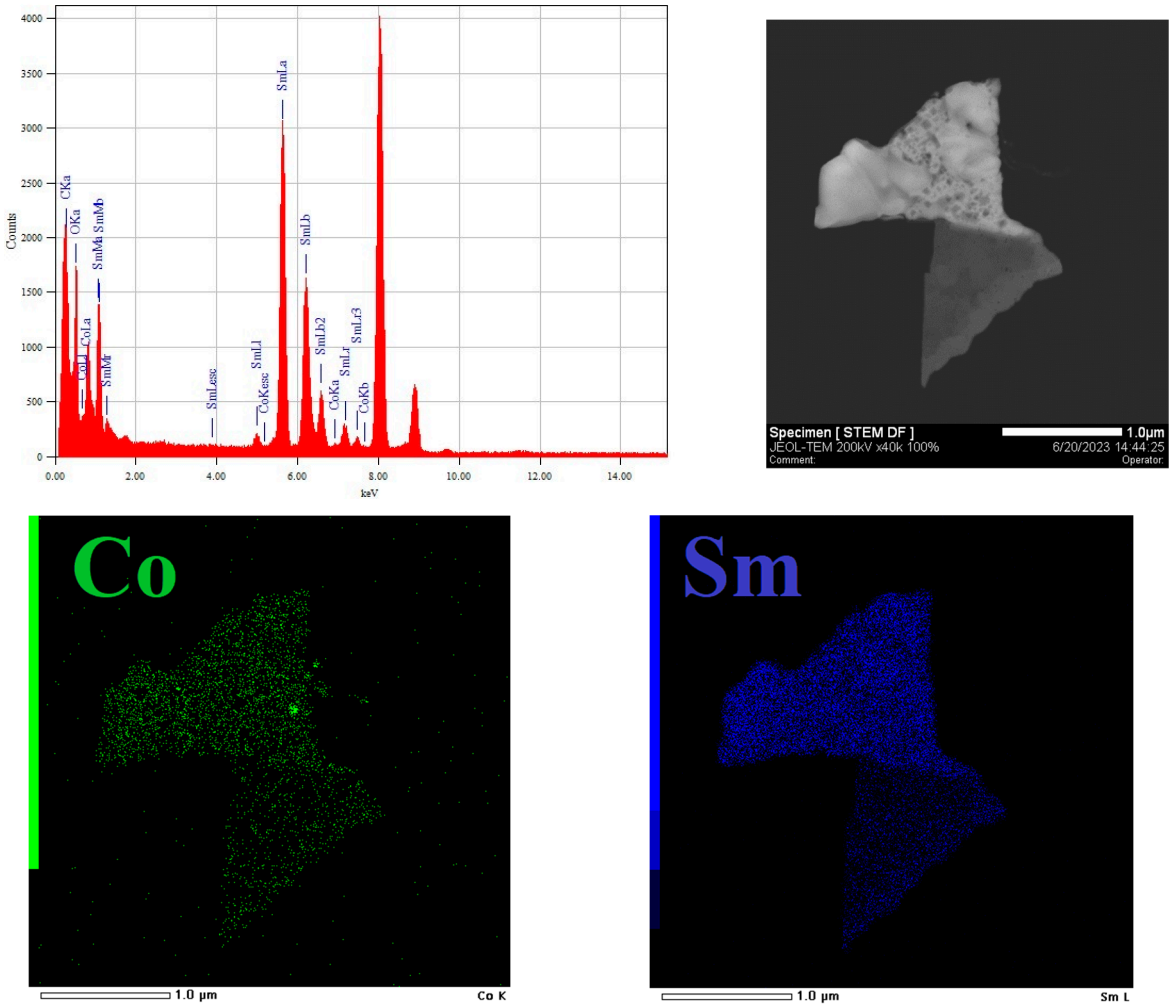

Figure 12. TEM images for the spent catalyst derived from 5% Co/Sm_2O_3: overall elemental spectra, STEM DF image, Co and Sm elemental maps.

An effective way to achieve high syngas yields using the synthesized precursors of catalysts was developed, which consists in heating samples in a nitrogen flow to an optimal temperature of 900 °C. This DRM procedure does not require catalyst pre-reduction by hydrogen or a CH_4/CO_2 mixture. The stable operation of the catalysts lasts for 50 h, and the yields of H_2 and CO close to the thermodynamically predicted limits are achieved.

It has been shown that the cobalt content in the pre-catalyst significantly affects the carbonization resistance of the formed DRM catalyst. For example, the catalyst derived from 2% Co/Sm_2O_3 is not subjected to carbonization when tested in DRM for 50 h. The catalysts based on 5% Co/Sm_2O_3 and 10% Co/Sm_2O_3 undergo noticeable carbonization, which, however, does not impair the results of DRM for 50 h. The 23% Co/Sm_2O_3 derived catalyst, which is similar in composition to $SmCoO_3$ perovskite, maintains stability in the DRM reaction for 50 h, but forms a significant amount of carbon. Such carburization will probably affect its stability during prolonged operation. Therefore, a cobalt content of 2 wt.% is optimal for obtaining the stable cobalt–samarium DRM catalyst, provided its preheating at 900 °C in a nitrogen flow is followed by the supply of reagents. The stability of this catalyst is associated with the formation of sintering-resistant metal cobalt particles with a size of approximately 20 nm. Similar observations were made in the study of DRM on supported nickel and nickel–cobalt catalysts containing not more than 2 wt.% of these metals [5,40].

4. Conclusions

A new simple method has been developed for the synthesis of materials that are effective precursors of catalysts for the production of hydrogen and carbon monoxide by DRM reaction.

It has been demonstrated that the formation of efficient and stable DRM catalysts based on the synthesized materials does not require their pre-reduction with hydrogen or the mixture of reagents. The heating of the synthesized materials at 900 °C in a nitrogen flow and the subsequent supply of the equimolar CH_4/CO_2 mixture make it possible to obtain in situ a selective and stable DRM catalyst operating for at least 50 h.

In general, a high cobalt content in the precursor of catalyst is not required to create a selective, stable, and carbonization resistant DRM catalyst. An increase in the cobalt content in the samples does not affect their stability for 50 h, but significantly increases carbonization, which may hinder a longer stable operation of DRM catalysts.

The catalyst formed from the 2% Co/Sm_2O_3 material is promising for practical use, since it is highly resistant to carbonization and the sintering of cobalt particles, and demonstrates high yields of H_2 and CO. Its application in the DRM reaction makes it possible to efficiently utilize two greenhouse gases, methane, and carbon dioxide, which is of great environmental importance. In addition, it can potentially be used to produce "green" hydrogen by the conversion of renewable raw material—biogas.

5. Patents

Russian Patent Application RU 2023 113 594 A (25 May 2023).

Supplementary Materials: The following supporting information can be downloaded at: https://www.mdpi.com/article/10.3390/pr11082296/s1, Figure S1: (a) XRD pattern of 2% Co/Sm_2O_3, (b) XRD pattern of 5% Co/Sm_2O_3, (c) XRD pattern of 10% Co/Sm_2O_3, (d) XRD pattern of 23% Co/Sm_2O_3; Figure S2: (a) XRD pattern of spent catalyst derived from 2% Co/Sm_2O_3, (b) XRD pattern of spent catalyst derived from 5% Co/Sm_2O_3, (c) XRD pattern of spent catalyst derived from 10% Co/Sm_2O_3, and (d) 23% Co/Sm_2O_3, (d) XRD pattern of spent catalyst derived from 23% Co/Sm_2O_3.

Author Contributions: Conceptualization, A.G.D. and A.S.L.; methodology, A.G.D. and A.S.L.; investigation, A.S.L., V.A.A., A.A.S., K.A.C. and G.A.S.; data curation, A.S.L., V.A.A. and M.A.B.; writing—original draft preparation, A.S.L.; writing—review and editing, A.S.L. and A.G.D.; supervision, A.G.D. and A.S.L.; funding acquisition, A.G.D. All authors have read and agreed to the published version of the manuscript.

Funding: This research was funded by Russian Science Foundation, grant number 23-13-00098. TGA, H2-TPR and SEM experiments were carried out within the state funding of TIPS RAS. SEM images were obtained at the IGIC RAS Joint Research Center for Physical Methods of Research.

Data Availability Statement: Russian Science Foundation, grant number 23-13-00098, https://rscf.ru/en/enprjcard?rid=23-13-00098 (accessed on 2 July 2023).

Conflicts of Interest: The authors declare no conflict of interest.

Abbreviations

DRM—dry reforming of methane; XRD—X-ray diffraction; SEM—scanning electron microscopy; TEM—transmission electron microscopy; H_2-TPR—temperature-programmed reduction; TGA—thermogravimetric analysis; syngas—synthesis gas, mixture of CO and H_2; POM—partial oxidation of methane; kJ—kilojoule; ΔH^0_{298}—standard enthalpy change; ΔG^0_{298} ≤—standard Gibbs energy change; T—temperature; h—hour; g—gram; m—meter; atm—atmosphere; BET—Brunauer–Emmett–Teller; S_{BET}—specific surface area; P—pressure; ICDD—International Center for Diffraction Data; kV—kilovolt; min—minute; mL—milliliter; mm—millimeter; L—liter; SE2—secondary electrons; ESB—energy selective backscattered electrons; REE—rare earth elements; wt.—weight; nm—nanometer; STEM—scanning transmission electron microscopy; DF—dark field.

References

1. Jang, W.-J.; Shim, J.-O.; Kim, H.-M.; Yoo, S.-Y.; Roh, H.-S. A review on dry reforming of methane in aspect of catalytic properties. *Catal. Today* **2019**, *324*, 15–26. [CrossRef]
2. Su, B.; Wang, Y.; Xu, Z.; Han, W.; Jin, H.; Wang, H. Novel ways for hydrogen production based on methane steam and dry reforming integrated with carbon capture. *Energy Convers. Manag.* **2022**, *270*, 116199. [CrossRef]
3. Singh, R.; Dhir, A.; Mohapatra, S.K.; Mahla, S.K. Dry reforming of methane using various catalysts in the process: Review. *Biomass Conv. Bioref.* **2020**, *10*, 567–587. [CrossRef]
4. Holmen, A. Direct Conversion of Methane to Fuels and Chemicals. *Catal. Today* **2009**, *142*, 2–8. [CrossRef]
5. Moiseev, I.I.; Loktev, A.S.; Shlyakhtin, O.A.; Mazo, G.N.; Dedov, A.G. New approaches to the design of nickel, cobalt, and nickel–cobalt catalysts for partial oxidation and dry reforming of methane to synthesis gas. *Petrol. Chem.* **2019**, *59* (Suppl. S1), S1–S27. [CrossRef]
6. Chen, L.; Qi, Z.; Zhang, S.; Su, J.; Somorjai, G.A. Catalytic Hydrogen Production from Methane: A Review on Recent Progress and Prospect. *Catalysts* **2020**, *10*, 858. [CrossRef]
7. Elbadawi, A.H.; Ge, L.; Li, Z.; Liu, S.; Wang, S.; Zhu, Z. Catalytic partial oxidation of methane to syngas: Review of perovskite catalysts and membrane reactors. *Catal. Rev.* **2021**, *63*, 1–67. [CrossRef]
8. Al-Sayari, S.A. Recent Developments in the Partial Oxidation of Methane to Syngas. *Open Catal. J.* **2013**, *6*, 17–28. [CrossRef]
9. Alhassan, M.; Jalil, A.A.; Nabgan, W.; Hamid, M.Y.S.; Bahari, M.B.; Ikram, M. Bibliometric studies and impediments to valorization of dry reforming of methane for hydrogen pro-duction. *Fuel* **2022**, *328*, 125240. [CrossRef]
10. Kumar, R.; Kumar, A.; Pal, A. Overview of hydrogen production from biogas reforming: Technological advancement. *Int. J. Hydrogen Energy* **2022**, *47*, 34831–34855. [CrossRef]
11. Bhattar, S.; Abedin, M.A.; Kanitkar, S.; Spivey, J.J. A review on dry reforming of methane over perovskite derived catalysts. *Catal. Today* **2021**, *365*, 2–23. [CrossRef]
12. The, L.P.; Setiabudi, H.D.; Timmiati, S.N.; Aziz, M.A.A.; Annuar, N.H.R.; Ruslan, N.N. Recent progress in ceria-based catalysts for the dry reforming of methane: A review. *Chem. Eng. Sci.* **2021**, *242*, 116606. [CrossRef]
13. Yentekakis, I.V.; Panagiotopoulou, P.; Artemakis, G. A review of recent efforts to promote dry reforming of methane (DRM) to syngas production via bimetallic catalyst formulations. *Appl. Catal. B Environ.* **2021**, *296*, 120210. [CrossRef]
14. Wang, C.; Wang, Y.; Chen, M.; Liang, D.; Yang, Z.; Cheng, W.; Tang, Z.; Wang, J.; Zhang, H. Recent advances during CH_4 dry reforming for syngas production: A mini review. *Int. J. Hydrogen Energy* **2021**, *46*, 5852–5874. [CrossRef]
15. Le Saché, E.; Reina, T.R. Analysis of dry reforming as direct route for gas phase CO_2 conversion. The past, the present and future of catalytic DRM technologies. *Prog. Energy Combust. Sci.* **2022**, *89*, 100970. [CrossRef]
16. Hambali, H.U.; Jalil, A.A.; Abdulrasheed, A.A.; Siang, T.J.; Gambo, Y.; Umar, A.A. Zeolite and clay based catalysts for CO_2 reforming of methane to syngas: A review. *Int. J. Hydrogen Energy* **2022**, *47*, 30759–30787. [CrossRef]
17. Baharudin, L.; Rahmat, N.; Othman, N.H.; Shah, N.; Syed-Hassan, S.S.A. Formation, control, and elimination of carbon on Ni-based catalyst during CO_2 and CH_4 conversion via dry reforming process: A review. *J. CO2 Util.* **2022**, *61*, 102050. [CrossRef]
18. Mortensen, P.M.; Dybkjær, I. Industrial scale experience on steam reforming of CO_2-rich gas. *Appl. Catal. A Gen.* **2015**, *495*, 141–151. [CrossRef]
19. Teuner, S.C.; Neumann, P.; Von Linde, F. The Calcor standard and Calcor economy processes. *OIL GAS Eur. Mag.* **2001**, *3*, 44–46. Available online: https://www.caloric.com/wp-content/uploads/2016/11/Caloric-Downloads-Calcor.pdf (accessed on 6 July 2023).
20. Usman, M.; Wan Daud, W.M.A.; Abbas, H.F. Dry reforming of methane: Influence of process parameters. A review. *Renew. Sustain. Energy Rev.* **2015**, *45*, 710–744. [CrossRef]
21. Schulz, L.A.; Kahle, L.C.S.; Delgado, K.H.; Schunk, S.A.; Jentys, A.; Deutschmann, O.; Lercher, J.A. On the coke deposition in dry reforming of methane at elevated pressures. *Appl. Catal. A Gen.* **2015**, *504*, 599–607. [CrossRef]
22. Jang, W.-J.; Jeong, D.-W.; Shim, J.-O.; Kim, H.-M.; Roh, H.-S.; Son, I.H.; Lee, S.J. Combined steam and carbon dioxide reforming of methane and side reactions: Thermodynamic equilibrium analysis and experimental application. *Appl. Energy* **2016**, *173*, 80–91. [CrossRef]
23. Yusuf, M.; Farooqi, A.S.; Keong, L.K.; Hellgardt, K.; Abdullah, B. Contemporary trends in composite Ni-based catalysts for CO_2 reforming of methane. *Chem. Eng. Sci.* **2021**, *229*, 116072. [CrossRef]
24. Jafarbegloo, M.; Tarlani, A.; Wahid Mesbah, A.; Sahebdelfar, S. Thermodynamic analysis of carbon dioxide reforming of methane and its practical relevance. *Int. J. Hydrogen Energy* **2015**, *40*, 2445–2451. [CrossRef]
25. Khoshtinat Nikoo, M.; Amin, N.A.S. Thermodynamic analysis of carbon dioxide reforming of methane in view of solid carbon formation. *Fuel Process. Technol.* **2011**, *92*, 678–691. [CrossRef]
26. Aziz, M.A.A.; Setiabudi, H.D.; Teh, L.P.; Annuar, N.H.R.; Jalil, A.A. A review of heterogeneous catalysts for syngas production via dry reforming. *J. Taiwan Inst. Chem. Eng.* **2019**, *101*, 139–158. [CrossRef]
27. Choudhary, V.R.; Mondal, K.C.; Mamman, A.S.; Joshi, U.A. Carbon-free dry reforming of methane to syngas over $NdCoO_3$ perovskite-type mixed metal oxide catalyst. *Catal. Lett.* **2005**, *100*, 271–276. [CrossRef]
28. Royer, S.; Duprez, D.; Can, F.; Courtois, X.; Batiot-Dupeyrat, C.; Laassiri, S.; Alamdari, H. Perovskites as Substitutes of Noble Metals for Heterogeneous Catalysis: Dream or Reality. *Chem. Rev.* **2014**, *114*, 10292–10368. [CrossRef]

29. Gavrikov, A.V.; Loktev, A.S.; Ilyukhin, A.B.; Mukhin, I.E.; Bykov, M.A.; Maslakov, K.I.; Vorobei, A.M.; Parenago, O.O.; Sadovnikov, A.A.; Dedov, A.G. Supercritical Fluid Assisted Modification combined with the Resynthesis of $SmCoO_3$ as Effective Tool to Enhance Long-term Performance of $SmCoO_3$-derived Catalysts for Dry Reforming of Methane to Syngas. *Dalton Trans.* **2022**, *51*, 18446–18461. [CrossRef]
30. Gavrikov, A.V.; Ilyukhin, A.B.; Belova, E.V.; Yapryntsev, A.D.; Dobrokhotova, Z.V.; Khrushcheva, A.V.; Efimov, N.N. Rapid preparation of $SmCoO_3$ perovskite via uncommon though efficient precursors: Composition matters! *Ceram. Int.* **2020**, *46*, 13014–13024. [CrossRef]
31. Osazuwa, O.U.; Cheng, C.K. Catalytic conversion of methane and carbon dioxide (greenhouse gases. into syngas over samarium-cobalt-trioxides perovskite catalyst. *J. Clean. Prod.* **2017**, *148*, 202–211. [CrossRef]
32. Salaev, M.A.; Liotta, L.F.; Vodyankina, O.V. Lanthanoid-containing Ni-based catalysts for dry reforming of methane: A review. *Int. J. Hydrogen Energy* **2022**, *47*, 4489–4535. [CrossRef]
33. De Lira Lima, D.C.; Lemos, I.P.; Gomes, R.S.; Rodrigues, L.M.T.S.; Fréty, R.T.; Resini, C.; Junior, R.B.S.; Brandão, S.T. Study of $LaNi_{1-x}Co_xO_3$ Perovskites-Type Oxides Either Pure or Mixed with SiO_2 as Catalytic Precursors Applied in CH_4 Dry-Reforming. *Catal. Lett.* **2023**, *153*, 2137–2148. [CrossRef]
34. Rietveld, H.M. A profile refinement method for nuclear and magnetic structures. *J. Appl. Crystallogr.* **1969**, *2*, 65–71. [CrossRef]
35. Olusola, J.O.; Sudip, M. Temperature programme reduction (TPR) studies of cobalt phases in γ-alumina supported cobalt catalysts. *J. Petrol. Technol. Altern. Fuels* **2016**, *7*, 1–12. [CrossRef]
36. Ma, F.; Chen, Y.; Lou, H. Characterization of perovskite-type oxide catalysts $RECoO_3$ by TPR. *React. Kinet. Catal. Lett.* **1986**, *31*, 47–53.
37. Dedov, A.G.; Loktev, A.S.; Ivanov, V.K.; Bykov, M.A.; Mukhin, I.E.; Lidzhiev, M.M.; Rogaleva, E.V.; Moiseev, I.I. Selective oxidation of methane to synthesis gas: Cobalt- and nickel-based catalysts. *Dokl. Phys. Chem.* **2015**, *461*, 73–79. [CrossRef]
38. Loktev, A.S.; Mukhin, I.E.; Bykov, M.A.; Sadovnikov, A.A.; Osipov, A.K.; Dedov, A.G. Novel high-performance catalysts for partial oxidation and dry reforming of methane to synthesis gas. *Pet. Chem.* **2022**, *62*, 526–543. [CrossRef]
39. Loktev, A.S.; Arkhipova, V.A.; Bykov, M.A.; Sadovnikov, A.A.; Dedov, A.G. Cobalt–Samarium Oxide Composite as a Novel High-Performance Catalyst for Partial Oxidation and Dry Reforming of Methane into Synthesis Gas. *Pet. Chem.* **2023**, *63*, 317–326. [CrossRef]
40. Dedov, A.G.; Loktev, A.S.; Mukhin, I.E.; Baranchikov, A.E.; Ivanov, V.K.; Bykov, M.A.; Solodova, E.V.; Moiseev, I.I. Effect of the Support Nature on Stability of Nickel and Nickel–Cobalt Catalysts for Partial Oxidation and Dry Reforming of Methane to Synthesis Gas. *Pet. Chem.* **2019**, *59*, 385–393. [CrossRef]